doi:10.1017/S1431927613004571
Microsc. Microanal. 19 (Suppl 2), 2013

3D Microstructural Analysis Using an *In Situ* Ultramicrotome (Gatan 3View™)

X. L. Zhong, T. Hashimoto, M.G.Burke and G. E. Thompson

School of Materials, University of Manchester, Manchester, UK

TEM tomography, MicroCT, Atom Probe, and FIB serial sectioning permit unique 3D characterisation of microstructure in contrast to conventional microscopy techniques. *In situ* ultramicrotome sectioning and BSE imaging (Serial Block Face(SBF) SEM) can provide the necessary meso-scale 3D data in terms of size and resolution, and the method complements the listed 3D techniques [1-2]. The original work of Denk *et al* (2004) and the work Leighton, who constructed a microtome for cutting sections inside an SEM in 1981, were developed commercially by Gatan (3View) in 2006 [3-4]. Over the past 5 years, the *in situ* ultramicrotome (Gatan 3View™) has attracted significant research activities in the biological sciences, but rather limited applications in materials science, particularly for metals research. In fact, the advantage of materials science applications, especially metals, is that no staining is needed. The strong Z contrast and weak topographical contrast of the backscattered electron images gives the 'flat' images suitable for 3D reconstruction. The 3D reconstruction is relatively simple and straightforward as it omits the process of making virtual slices as used for X-ray or TEM projection tomography. Further, it is a relatively easy operation as compared with TEM and FIB reconstructions.

Three representative material applications are presented here. Figure 1 shows the 3D microstructure and corrosion product produced on a Sn-0.7Cu lead-free solder after an immersion test in 3.5% NaCl solution. The dissolution of Sn is evident. The Cl^- ions promote the dissolution of Sn [5]. For this work, each ultramicrotomed slice was 10 nm thickness, and the cutting speed was set at 0.1mm/s to minimise heat generation. Cutting speed, clearance angle, slice thickness, size of block-face, knife solid angle and the electron beam energy are the main factors affecting the quality of the results and the heat generation.

Figure 2 shows the 3D characterization of aluminium alloy AA2024 and magnesium alloy WE43. This technique clearly revealed the 'true' porosity and spatial distribution of intermetallic particles in A2024 aluminium alloy. The size, morphology and 3D distribution of intermetallics in magnesium alloy WE43 are evident in the reconstructed volume. The cutting speed for these analyses was set at 1mm/s. The thickness of each slice was 20 nm and 25m for the aluminium alloy and magnesium alloy, respectively. The BSE images were obtained at 2 keV for these three specimens. It was observed that cutting thick slices could reduce the temperature increase in the block face, which appears to be due to the removal of the hottest top surface from the bulk materials. The correlation between the SEM voltage for imaging and the thickness of the slice must be considered in order to obtain correct data from SBFSEM (Figure 3). The source of the collected (imaged) backscattered electrons must be considered in order to appropriately match the cutting thickness with beam voltage since electron trajectories in each specimen are determined by the applied voltages. Monte Carlo simulation indicates that not many materials have a backscattered electron generation region of less than 5 nm from the surface, even at 1keV. Additionally, setting a slice thickness that is too thin (especially below 5-10 nm), may lead to non-uniform slices throughout the sectioning process due to the design of the ultramicrotome. Our experience has demonstrated that 'soft metals' like aluminum alloys, magnesium alloys, zinc alloys, and solder alloys are good candidates for this novel serial-sectioning technique.

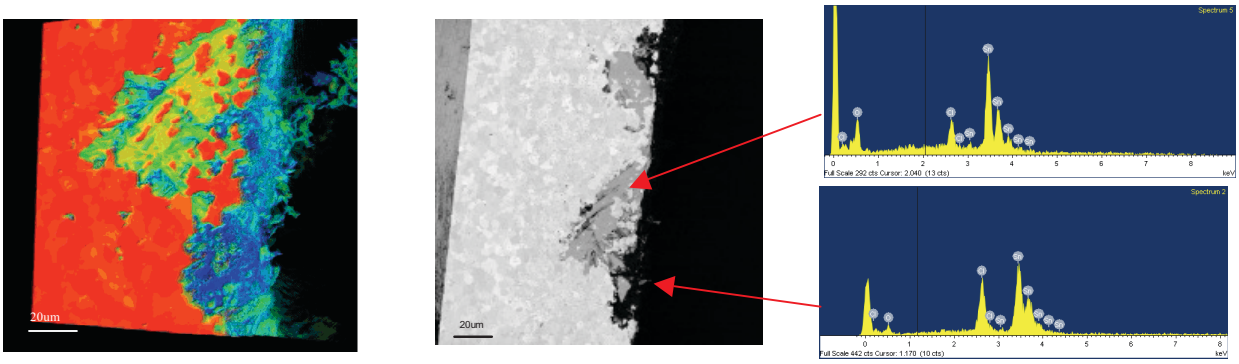

(a) (b) (c)

Figure 1. Corrosion of Sn-0.7Cu alloy: (a) 3D view of the corrosion area; (b) block-face after the ultramicrotome slice; (c) EDX results showing a Sn-Cl-O compound that formed in the corrosion pits.

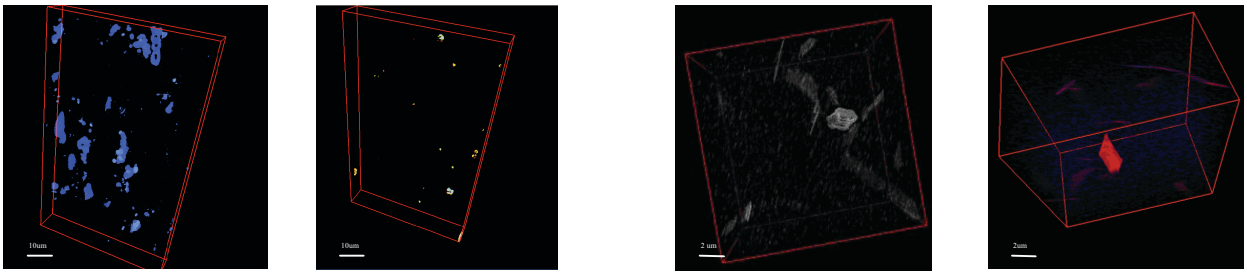

(a) (b) (c) (d)

Figure 2. 3D characterization of A2024 aluminum alloy and WE43 magnesium alloy: (a) 3D distribution of A2024 intermetallic particles; (b) 3D distribution of the pores in A2024; (c) 3D spatial distribution (shape, size and location) of intermetallics in WE43; (d) segmentation of WE43.

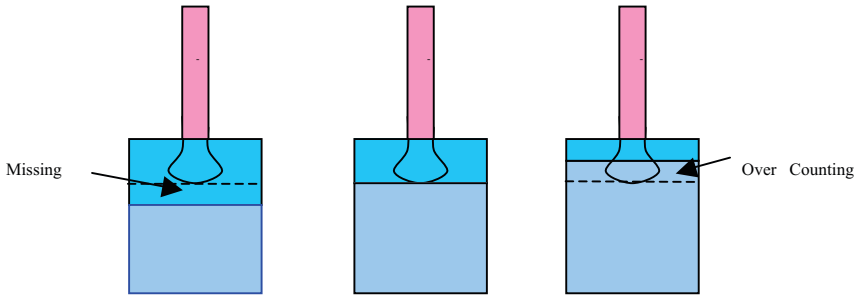

(a) (b) (c)

Figure 3. Correlation of e-beam energy and section thickness, (a) inadequate (low) e-beam energy; (b) good correlation of e-beam energy and section thickness, (c) excessive (high) e-beam energy.

References:

[1] Scott K., J. Microsc. **242** (2010). p. 86-93.
[2] Möbus G. and Inkson B.J. Materials Today **10**, (2007). p. 18-25
[3]Denk W, Horstmann H, PLoS Biol **2(11):** e329. (2004)
[4] Leighton SB, Scan Electron Microsc **2** (1981) p. 73–76.
[5] F. Rosalbino, E. Angelini, G. Zanicchi, R. Carlini,and R. Marazza, Electrochmica Acta, **54**, (2009), p. 7231-7235

https://doi.org/10.1017/S1431927613004571 Published online by Cambridge University Press